Molecular Catalysis xxx (xxxx) xxx

Contents lists available at ScienceDirect

Molecular Catalysis

journal homepage: www.journals.elsevier.com/molecular-catalysis

Roles of supports on reducibility and activities of Cu_3P catalysts for deoxygenation of oleic acid: *In situ* XRD and XAS studies

Nopparuj Kochaputi [a], Pongtanawat Khemthong [b,c,*], Panita Kasamechonchung [b], Teera Butburee [b,c], Wanwisa Limphirat [d], Yingyot Poo-arporn [d], Sanchai Kuboon [b,c], Kajornsak Faungnawakij [b,c], Chanapa Kongmark [a,c,**]

[a] Department of Materials Science, Faculty of Science, Kasetsart University, Bangkok, 10900, Thailand
[b] National Nanotechnology Center (NANOTEC), National Science and Technology Development Agency (NSTDA), Pathum Thani, 12120, Thailand
[c] Research Network of NANOTEC – KU on NanoCatalysts and NanoMaterials for Sustainable Energy and Environment, Thailand
[d] Synchrotron Light Research Institute, 111 University Avenue, Muang, Nakhon Ratchasima, 30000, Thailand

ARTICLE INFO

Keywords:
Deoxygenation
Oleic acid
Cu_3P
In situ XRD
In situ XAS

ABSTRACT

This work demonstrates for the first time that SiO_2 and ultra-stable zeolite Y (USY) supports play significant roles in the reducibility of $Cu_2P_2O_7$ to form Cu_3P, which consequently affects the selectivity of oleic acid deoxygenation. The formation of supported Cu_3P nanoparticles during hydrogen reduction of $Cu_2P_2O_7$ was carefully investigated by *in situ* X-ray diffraction (*in situ* XRD), and *in situ* X-ray absorption spectroscopy (*in situ* XAS). The results indicate that the transformation of $Cu_2P_2O_7$ to Cu_3P occurs through several steps. In the first step, all supported $Cu_2P_2O_7$ precursors are reduced to metallic Cu. Then, copper particles on SiO_2 support react with phosphorus compounds and directly transform to Cu_3P. On the other hand, copper particles on USY support partially transform to CuP_2 and $Cu(OH)_2$ before all converting to Cu_3P. Despite multi-step transformations, $Cu_2P_2O_7$/USY exhibits the lowest onset reduction temperature and provides Cu_3P with a small particle size. The deoxygenation of oleic acid over Cu_3P supported catalysts reaches nearly 100 % conversion. Both catalysts favor cyclization and aromatization to form cyclic and aromatic compounds. Cu_3P/SiO_2 achieves higher dodecylbenzene yield (46 %) than Cu_3P/USY (33 %). A proposed mechanism consists of hydrogenation of oleic acid and deoxygenation, then followed by cracking, cyclization, aromatization, and alkyl rearrangement.

1. Introduction

Deoxygenation (DO) of oxygenated compounds over transition metal phosphides have received considerable attention in recent years owing to their excellent catalytic activity and stability under hydrotreatment conditions [1,2]. Various supported metal phosphides including WP, MoP, Ni_2P, Co_2P and Cu_3P have been used for removing oxygen atoms from oxygenated hydrocarbons [3–7]. Among these metal phosphides, Cu_3P seems to be less explored. Recently, it was reported that Cu_3P shows metal-like catalytic behaviors with high catalytic activity and excellent hydrogen adsorption-desorption ability [7,8]. Cu_3P has also been used as an electrocatalyst for the hydrogen evolution reaction (HER) under both acidic and basic conditions [9,10]. Its high electrical conductivity and chemical stability are also beneficial for electrochemical applications. Besides, Soták et al. reported the potential use of carbon supported Cu_3P catalysts for hydrogenolysis of biomass-derived alcohols such as glucose, sorbitol, and xylitol [11]. Indeed, supported Cu_3P catalysts have been shown to have a good catalytic activity for fatty acid deoxygenation [7].

Great efforts have been dedicated for preparation of Cu_3P with desired properties using various synthetic approaches such as colloidal methods [12,13], solvothermal synthesis [14,15], solid-state reaction [14,16], and reduction methods in H_2 atmosphere [11]. Well-dispersed metal phosphide nanoparticles on supports are desirable for catalytic applications. In general, hydrogen reduction of metal precursors (*e.g.*, metal phosphates/phosphites/hypophosphites or a mixture of metal salt/oxide and phosphorus compounds) deposited on the pore walls of supports by aqueous impregnation would allow the formation of metal

* Corresponding author at: National Nanotechnology Center (NANOTEC), National Science and Technology Development Agency (NSTDA), Pathum Thani, 12120, Thailand.
** Corresponding author at: Department of Materials Science, Faculty of Science, Kasetsart University, Bangkok, 10900, Thailand.
E-mail addresses: pongtanawat@nanotec.or.th (P. Khemthong), chanapa.k@ku.th (C. Kongmark).

https://doi.org/10.1016/j.mcat.2021.111425
Received 30 September 2020; Received in revised form 2 January 2021; Accepted 18 January 2021
2468-8231/

phosphide particles dispersed on a support material [1,4]. Typically, this method requires high temperatures (~ 500 – 1000 °C) and hydrogen atmosphere for the reduction of the metal precursors. Although hydrogen reduction is an important process for the production of highly active metal phosphides, only a few studies have been carried out for FeP, Ni_2P, Ni_3P, $Ni_{12}P_5$, CoP, MoP and WP [1,4,17]. Their results suggest that the reduction of phosphate or phosphite compounds mostly occurs through the formation of metal particles which later react with phosphorus species and transform to metal phosphide particles. However, metal phosphide particles can also be formed by other routes. For example, proved by *in situ* X-ray diffraction (XRD) and X-ray absorption spectroscopy (XAS) techniques, Berhault et al. reported that ammonium nickel phosphate $NiNH_4PO_4{\cdot}H_2O$ can be reduced to nickel phosphide *via* an amorphous intermediate phase [18]. Time-resolved XRD results reported by Rodriguez et al. illustrated the formation of Ni_2P/SiO_2 catalyst through Ni and $Ni_{12}P_5$ intermediates which were not detected in the unsupported catalyst [19]. It is well known that the catalyst support plays an important role on the reduction of metal precursors, the structure of active phases and the catalytic activity [20]. To the best of our knowledge, there are no reports on the formation mechanism of supported Cu_3P catalysts using hydrogen reduction method. Details of these reduction pathways remain unclear. Therefore, a comprehensive study on the formation mechanism of Cu_3P nanoparticles on various supports during hydrogen reduction process is essential for the optimization of this material for catalytic applications.

As demonstrated in our previous report [7], the catalyst supports (USY, Al_2O_3, and SiO_2) significantly influence the activity and product selectivity of the Cu_3P catalyst. Therefore, in the present work, we aim to further clarify the roles of the supports on the catalytic behavior of the Cu_3P. Based on the assumption that a different support could induce the formation of different copper species during hydrogen reduction process, we carefully investigate those phase transformation processes.

Thus, in this study, we prepared copper pyrophosphate precursor ($Cu_2P_2O_7$) supported on SiO_2 and ultra-stable zeolite Y (USY) by impregnation method using metal salts and ammonium phosphate. The formation of copper phosphide (Cu_3P) by hydrogen reduction of $Cu_2P_2O_7$ was monitored by *in situ* X-ray diffraction (XRD) and X-ray absorption spectroscopy (XAS) techniques. The combination of *in situ* XRD and *in situ* XAS provided information of both short-range and long-range structural modifications, which allow us to understand crystallization processes and effects of the catalyst supports on the formation mechanism. This is regarded as one of the most powerful methods to determine the nature of intermediate phases formed during the synthesis and to optimize the conditions for the production of supported Cu_3P nanoparticles. The catalytic performance was demonstrated for oleic deoxygenation (DO) reaction. We believe that this insightful investigation would reveal the evolving intrinsic activities and materials properties as a function of catalyst supports. This will be essential for understanding reduction behaviors and catalytic mechanisms of the supported catalysts.

2. Experimental section

2.1. Catalyst preparation

Synthesis of the supported Cu_3P catalysts was based on hydrogen reduction of supported copper pyrophosphate ($Cu_2P_2O_7$) precursors. First, the supported $Cu_2P_2O_7$ precursors (10 wt.% Cu) were prepared by incipient wetness impregnation method using an aqueous solution containing $Cu(NO_3)_2$ and $(NH_4)_2HPO_4$ with the Cu/P molar ratio of 2:1 under constant stirring. A few drops of nitric acid were added to dissolve some precipitates until a clear light blue solution was obtained. Then, the prepared solution was impregnated on SiO_2 or ultra-stable zeolite Y (USY) supports. These impregnated samples were dried at 80 °C for 12 h and calcined under air atmosphere at 450 °C for 3 h, resulting in light blue powders which were referred as $Cu_2P_2O_7/SiO_2$ and $Cu_2P_2O_7$/USY precursors. Finally, those calcined samples were further reduced under hydrogen atmosphere at 650 °C for 5 h to obtain Cu_3P/SiO_2 and Cu_3P/USY catalysts.

2.2. Characterization of the supported Cu_3P catalysts

The structural evolution during the hydrogen reduction of $Cu_2P_2O_7$ to Cu_3P was studied by *ex situ* and *in situ* XRD (D8 ADVANCE, Bruker, Ltd.) using Cu Kα radiation with Ni filter, operated at 40 kV and 40 mA, in the 2θ range of 10 – 80°. The supported $Cu_2P_2O_7$ precursor was put on a Pt-Rh alloy plate in a heating cell chamber which was later heated from 50 °C to 650 °C with a heating rate of 0.1 °C s^{-1} under hydrogen flow (20 mL min^{-1}) and hold at 650 °C for 45 min. The diffraction pattern was acquired at a regular interval (every 50 °C) by the same powder diffractometer that was used at room temperature measurements. LaB_6 was used as a standard to determine the instrumental resolution of the X-ray diffractometer.

The morphology and dispersion of Cu_3P catalyst on different supports were determined by scanning electron microscopy (HITACHI SU5000 FE-SEM) in backscattered electron (BSE) mode with an acceleration voltage of 10 kV.

Temperature-programmed reduction profiles were performed on a TPR automated chemisorption analyzer (ChemBET Pulsar, Quantachrome). Each 100 mg of calcined samples was pretreated under helium atmosphere at 120 °C for 1 h. Subsequently, the samples were then reduced under H_2/Ar mixture (H_2/Ar = 1.5; total flow 30 cm^3 min^{-1}) and heated from 100 to 800 °C with a heating rate of 5 °C min^{-1}.

The evolution of the valence state, geometry, and Cu species during hydrogen reduction was monitored by *in situ* XAS. Cu K-edge XAS experiments were performed in transmission mode, at the Time-resolved XAS beamline (BL2.2) of the Synchrotron Light Research Institute (SLRI) in Thailand. A bent crystal Si (111) in the energy dispersive monochromator was used to focus a polychromatic X-ray beam onto the sample. The X-rays pass through the sample and diverge towards a position-sensitive detector (NMOS-linear image sensor). The experiments were carried out in a specially designed high temperature cell [21]. Each supported $Cu_2P_2O_7$ precursor was pressed into a pellet and loaded into the cell. Then it was reduced in 75 %H_2 in N_2 (total flow rate of 20 mL min^{-1}) at 650 °C for 30 min with a heating rate of 2 °C min^{-1}. The obtained XAS data were processed using the Athena graphical interface of the IFEFFIT program suite [22]. A combination of principal component analysis (PCA) and linear combination fit (LCF) analysis were applied on the normalized XANES spectra in the $-20\ eV < E_0 < 90\ eV$ range.

2.3. Catalytic deoxygenation of oleic acid

Oleic acid was used as a model compound for deoxygenation (DO) reaction. The reaction was carried out in a Parr batch reactor. Approximately 1 g of supported metal phosphide catalyst and 60 mL of a 5 wt% solution of oleic acid in dodecane were loaded into the reactor. Prior to the reaction, the reactor was purged with N_2, then heated to 340 °C and held at this temperature for 6 h. The liquid products were analyzed by a gas chromatograph equipped with a mass spectrometer (GC–MS). The DB-1HT was used as a capillary column. In addition, the gas-phase products were not further analyzed because methanation and water gas shift reaction were involved as the main gas phase reaction. The conversion of oleic acid was calculated according to the following equations.

$$\text{conversion}\ (\%) = \frac{\text{initial mole of oleic acid} - \text{final mole of oleic acid}}{\text{initial mole of oleic acid}} \times 100 \quad (1)$$

The selective yield (Y) of products were calculated based on carbon mass balance [23]

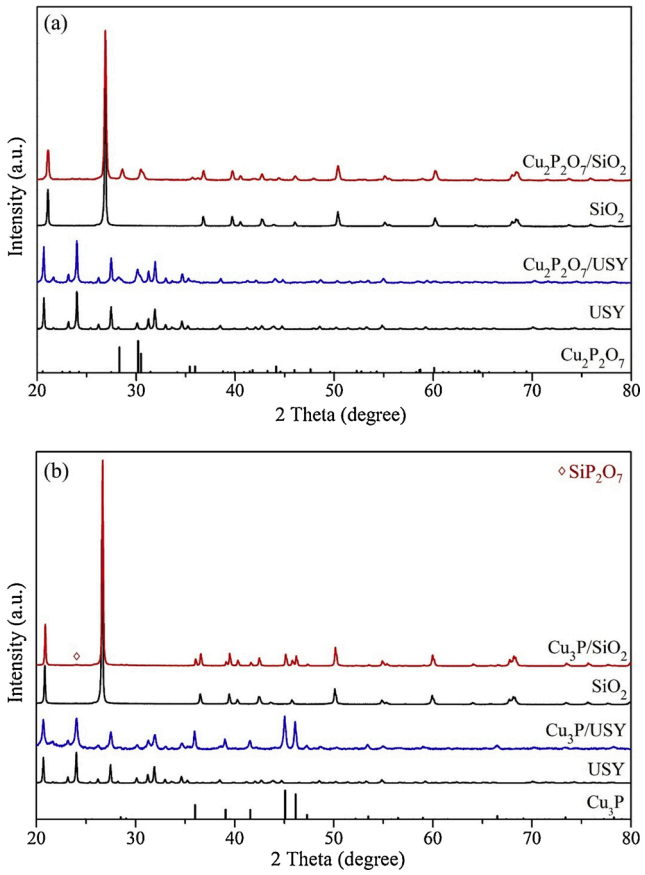

Fig. 1. XRD patterns of (a) calcined catalysts and (b) reduced catalysts with supports.

$$Y_i\ (\text{mol}\ \%) = \left(\frac{n_i \times a_i}{n_{Oleic\ acid} \times a_{Oleic\ acid}}\right) \times 100 \quad (2)$$

Where n_i and a_i represent the mole and carbon atom number of product *i*. $n_{Oleic\ acid}$ and $a_{Oleic\ acid}$ represent the mole and carbon atom number of oleic acid. The qualitative and quantitative analyses were conducted on HDO and DCO/DCO_2 products. The unspecified liquid products could be referred to as cyclic or aromatic compounds and polymerized products.

3. Results and discussion

3.1. Structures and morphologies

The crystal structure of the supports and the calcined catalysts were confirmed by means of *ex situ* XRD and presented in Fig. 1a. All samples exhibit characteristic lines of α-$Cu_2P_2O_7$ monoclinic structure with *C*2/*c* space group (PDF no. 00-044-0182) at 28.3°, 30.2° and 30.5°. The low intensity of $Cu_2P_2O_7$ lines is observed due to the low metal concentration. After the reduction in hydrogen atmosphere at 650 °C for 5 h, all catalysts show the characteristic diffraction peaks of Cu_3P hexagonal structure with $P6_3cm$ space group (PDF no. 01-071-2261) at 36.0°, 39.1°, 41.6°, 45.1°, 46.2° and 47.3°, as illustrated in Fig. 1b. There is no characteristic peaks of impurities observed in Cu_3P/USY catalysts. In the XRD pattern of Cu_3P/SiO_2 catalyst, a small additional peak is noticed at 24.1° which can be attributed to SiP_2O_7 phase (PDF no. 01-070-2245). Tiberius et al. also found the formation of SiP_2O_7 during the thermal dehydration of $Ca(H_2PO_4)_2{\cdot}H_2O$–SiO_2 system [24]. It was suggested that H_3PO_4 occurred during the reaction reacted with the SiO_2 and yielded SiP_2O_7. The crystallite sizes of Cu_3P catalysts, estimated from the XRD peak width by using the Debye Scherrer equation, are 80.4 and 42.1 nm for SiO_2 and USY supports, respectively. The Cu_3P catalyst particles on USY support are about half the size of those on SiO_2 support.

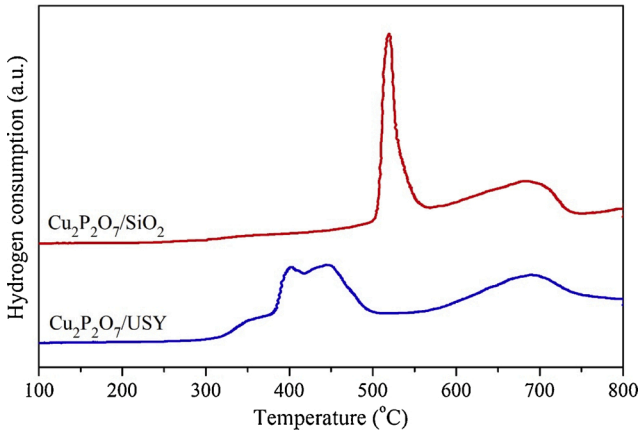

Fig. 3. H_2-TPR profiles of $Cu_2P_2O_7$ precursor on SiO_2 and USY supports.

The morphologies of supported Cu_3P catalysts are illustrated in Fig. 2. Backscattered electron images show specimen contrast caused by variation of atomic weights. The brighter areas are Cu_3P particles deposited on each support. Note that Cu_3P particles are well dispersed on the USY support (Fig. 2b) with a homogeneous particle size of less than 100 nm, while those on SiO_2 support (Fig. 2a) form agglomerates with diameters ranging from 50 to 500 nm.

3.2. Reduction behaviors

Hydrogen temperature-programmed reduction (H_2-TPR) experiments were performed to investigate the reduction behavior of $Cu_2P_2O_7$ supported on SiO_2 and USY. Fig. 3 shows the evolution of hydrogen consumption during the reduction process. To the best of our knowledge, our present work is the first report on TPR studies for copper phosphide catalysts which are synthesized by reduction of phosphate

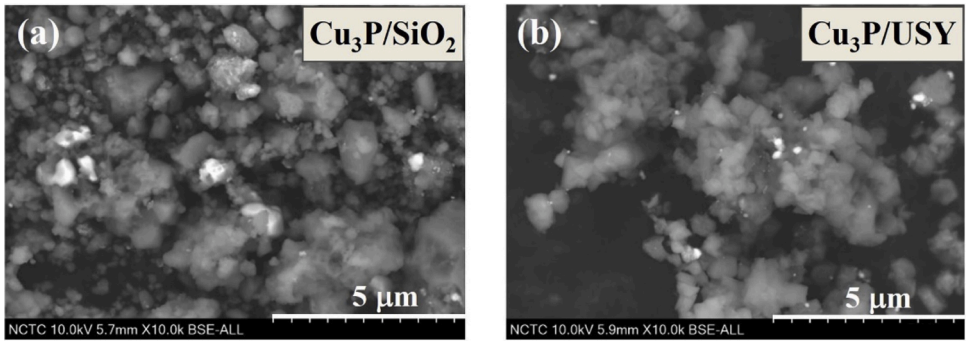

Fig. 2. Back scattered SEM images of Cu_3P catalyst on (a) SiO_2 and (b) USY supports.

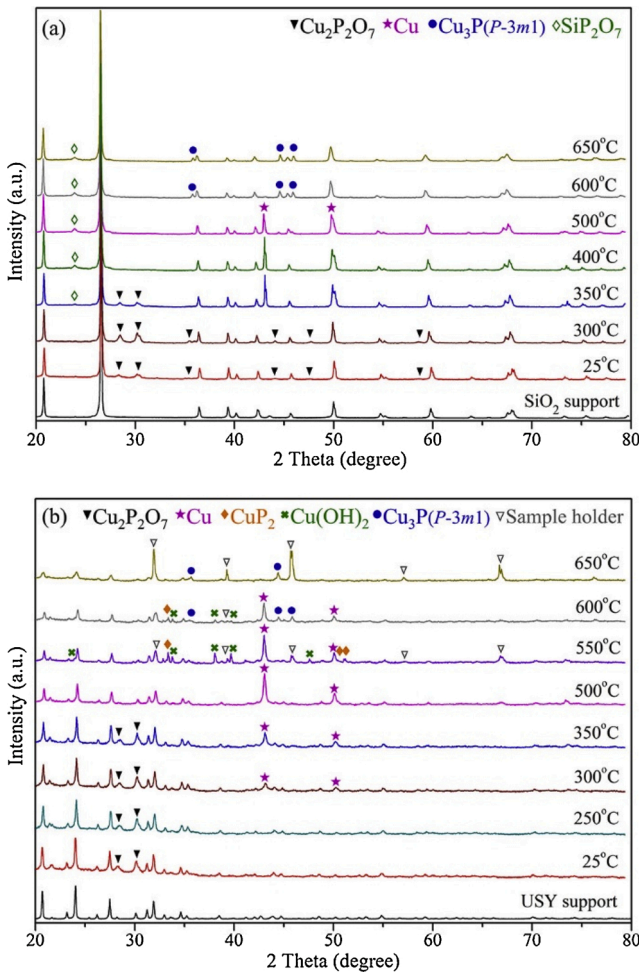

Fig. 4. XRD patterns collected during hydrogen reduction of $Cu_2P_2O_7$ precursor on (a) SiO_2 and (b) USY supports.

precursors on different supports. A few H_2-TPR studies were conducted on other metal phosphide catalysts (*e.g.*, FeP, Ni_2P, CoP, MoP and WP) [1,17,25]. Although each catalyst shows a specific TPR profile (composed of a single peak or several overlapping peaks), it was suggested that most of metal phosphides follow a similar reduction process. The partly or completely reduced transition metal promotes the reduction of phosphite or phosphate components to volatile phosphorus compounds such as phosphine (PH_3), H_3PO_4, H_3PO_3 or H_3PO_2 that react with reduced metals to form transition metal phosphides. As shown in Fig. 3, the TPR profiles of Cu_3P/SiO_2 catalyst consist of a strong hydrogen uptake peak at 530 °C and a weak broad peak at around 690−760 °C, while the Cu_3P/USY catalyst shows three unresolved peaks at 360, 403 and 445 °C and a broad peak at 690 °C. The hydrogen reduction process of the catalyst supported on USY seems to be more complex and takes place at lower temperature than that on SiO_2 support. The hydrogen reduction mechanism of $Cu_2P_2O_7$ to Cu_3P on catalyst supports is still unclear. Therefore, the structural evolution behind these reduction processes were further studied in detail by *in situ* XRD and *in situ* XAS.

3.3. Formation mechanisms of supported Cu_3P catalysts

In situ high-temperature XRD patterns collected during hydrogen reduction of $Cu_2P_2O_7$ precursor on SiO_2 and USY supports from room temperature to 650 °C are illustrated in Fig. 4a and b, respectively. The $Cu_2P_2O_7/SiO_2$ and $Cu_2P_2O_7$/USY precursors exhibit different reduction behaviors. At the beginning of the reaction, a crystalline phase of

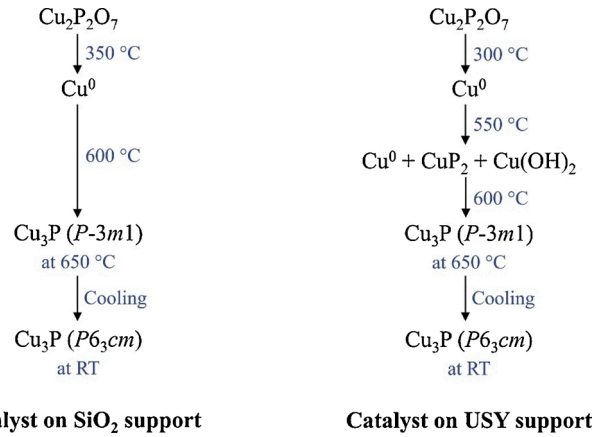

Fig. 5. Reduction mechanisms of $Cu_2P_2O_7$ precursors on SiO_2 and USY supports to Cu_3P catalysts deduced from *in situ* XRD data.

$Cu_2P_2O_7$ and corresponding supports are observed at room temperature. When $Cu_2P_2O_7/SiO_2$ is heated up to 300 °C, the intensity of $Cu_2P_2O_7$ lines slightly increases due to a higher degree of crystallinity. At 350 °C, the characteristic lines of Cu are noticed (*Fm*-3*m*, PDF no. 01-089-2838). Cu lines become stronger and reach the maximum intensity at 400 °C while the $Cu_2P_2O_7$ precursorvanishes, indicating the complete reduction of $Cu_2P_2O_7$ to metallic Cu. At 500 °C, the diffraction peaks attributed to Cu_3P (*P*-3*m*1 with PDF no. 03-065-1973) emerge while those of Cu gradually disappear, suggesting the transformation from metallic Cu to Cu_3P structure. The pure crystalline phase of Cu_3P (*P*-3*m*1) is successfully obtained at 650 °C. This high temperature trigonal form of Cu_3P is later stabilized in hexagonal polymorph ($P6_3cm$) at room temperature [26,27], which is in line with the *ex situ* XRD studies. In addition, a small characteristic peak of SiP_2O_7 is observed ($2\theta \sim 23.9°$) in the diffraction patterns of silica-supported catalyst at temperatures above 300 °C. The formation of SiP_2O_7 can occur on the surface of silica-supported metal phosphide catalyst with an excess phosphorus or metal phosphide content [24]. This is in accordance with the *ex situ* XRD results. The diffraction peaks of Pt-Rh alloy contributed from the sample holder can also be observed at high temperature due to the sintering shrinkage of the sample.

The structural evolution during the reduction of $Cu_2P_2O_7$ on USY

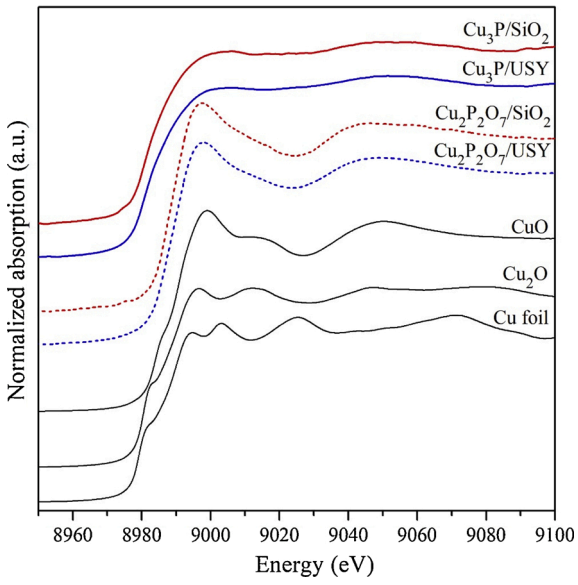

Fig. 6. XANES spectra of Cu references, $Cu_2P_2O_7$ precursors and Cu_3P catalysts on SiO_2 and USY supports.

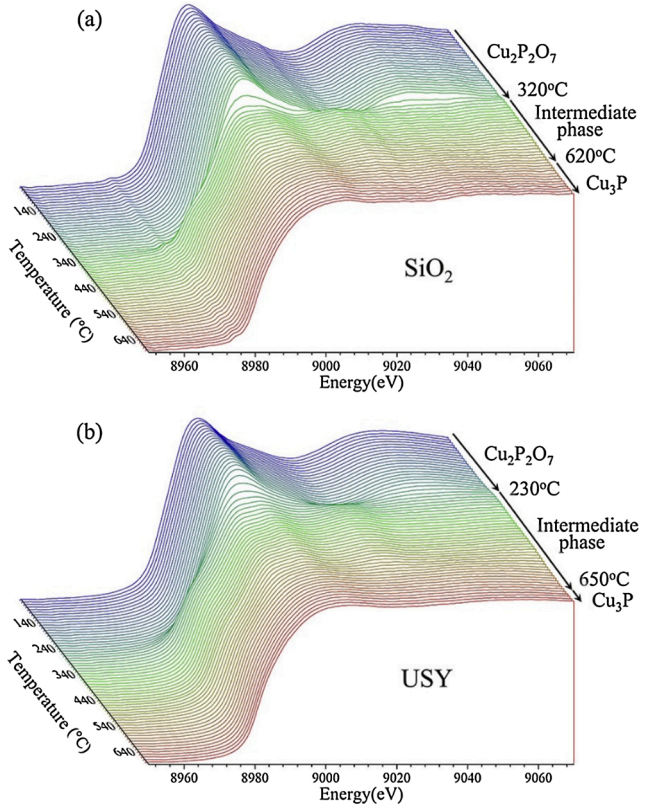

Fig. 7. Stacked plots of XANES spectra of (a) $Cu_2P_2O_7/SiO_2$ and (b) $Cu_2P_2O_7$/USY precursors during hydrogen reduction.

(Fig. 4b) appears differently from that on SiO_2 support. By increasing the temperature to 300 °C, the characteristic peaks of an intermediate metallic Cu phase emerge and grow at the expense of $Cu_2P_2O_7$ which gradually disappears at 500 °C. This result is in good agreement with the H_2-TPR profiles which show that $Cu_2P_2O_7$ on USY support is reduced to metallic Cu at lower temperatures than that on SiO_2 support. Afterward, the metallic Cu possibly reacts with hydrogen, water and the remaining phosphorus compounds, such as gaseous PH_3 or H_3PO_4 [1,4,17,24,25] that cannot be detected by XRD, to form intermediate phases including CuP_2 ($P2_1/c$, PDF no. 00-055-0400) and $Cu(OH)_2$ (*Cmcm*, PDF no. 00-035-0505) at 550 °C. These intermediate phases later transform to Cu_3P ($P\text{-}3m1$) upon heating to 650 °C. The Cu_3P on USY support is later stabilized in the most stable polymorphic form, *i.e.*, a hexagonal structure with $P6_3cm$ space group at room temperature, as previously evidenced by *ex situ* XRD studies [26,27]. The reduction mechanisms of $Cu_2P_2O_7$ to Cu_3P catalyst on SiO_2 and USY supports deduced from XRD results are summarized in Fig. 5.

Furthermore, the evolution of the valence state and local atomic structure of copper in the catalysts during hydrogen reduction was studied by *in situ* XAS. Fig. 6 presents Cu K-edge XANES (X-ray absorption near edge structure) spectra of supported $Cu_2P_2O_7$ precursors and Cu_3P catalysts at room temperature together with the spectra of reference materials, *i.e.*, Cu foil, Cu_2O and CuO. XANES spectrum of each reference material exhibits specific features, *i.e.*, edge energy, pre-peak, white line peak and oscillation shape, because they are sensitive to the oxidation state and local structure around the copper atoms. Cu^0, Cu^+ and Cu^{2+} exhibit absorption edges at 8979, 8981 and 8984 eV, respectively [28]. The absorption edge of supported $Cu_2P_2O_7$ samples correlate well with that of CuO, suggesting the presence of Cu(II) ions. Note that the dissimilarity in shoulder feature at 8986 eV (attributed to $1s \rightarrow 4p_{xy}$ electronic transition) between CuO and $Cu_2P_2O_7$ precursor is related to the difference in copper ion coordination and covalency of the equatorial ligands [29]. All supported $Cu_2P_2O_7$ precursors exhibit a white line

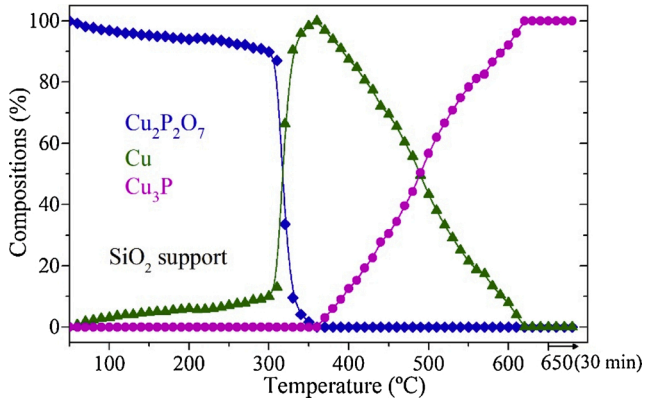

Fig. 8. Composition of the Cu species at different reaction times calculated by linear combination fitting (LCF) of the XANES spectra recorded during hydrogen reduction of $Cu_2P_2O_7/SiO_2$.

feature at 9001 eV and a similar oscillatory structure. No evidence of the characteristic features from either Cu_2O or CuO is observed in XANES spectra of the precursors and the catalysts, which would affirm the absence of copper oxide traces in all of our samples. Regarding to the supported Cu_3P catalysts, they exhibit identical edge energy and oscillatory structure. Their absorption edge energy significantly shifts to lower energy (~ 8981 eV) due to a decrease in the oxidation states of Cu from Cu^{+2} to Cu^{+1} after hydrogen reduction. Comparing XANES spectra of Cu_3P and Cu_2O standard at the absorption edge region, Cu_2O with linear 2-coordinate Cu(I) complex shows a shoulder feature at 8983 eV corresponding to $1s \rightarrow 4p_{xy}$ electronic transition which is not observed in the 4-coordinate tetrahedral Cu(I) complex of Cu_3P [29–31]. Therefore, these XAS results would confirm $Cu_2P_2O_7$ structure for the calcination step and Cu_3P structure for the reduction step, as previously shown in the XRD results.

Stacked plots of time resolved Cu K-edge XANES spectra of $Cu_2P_2O_7$ on SiO_2 and USY supports during hydrogen reduction from room temperature to 650 °C are given in Fig. 7a and 7b, respectively. The two samples exhibit dissimilar structural evolution. For $Cu_2P_2O_7/SiO_2$, principal component analysis indicates three different species involved in this reaction, including $Cu_2P_2O_7$, Cu^0 and Cu_3P. Linear combination fit (LCF) analysis of XANES spectra provides the evolution of the relative abundances of copper species during hydrogen reduction of $Cu_2P_2O_7/SiO_2$ (shown in Fig. 8). $Cu_2P_2O_7$ is reduced to metallic Cu at temperatures above 310 °C. This is shown in a gradual decrease of the absorption edge from ~ 8987 to ~ 8979 eV, together with a decrease in white line intensity. The maximum amount of Cu0 intermediate phase is observed at 360 °C. Further heating causes a shift in absorption edge energy from ~ 8979 to ~ 8981 eV, a decrease in white line intensity, and an alteration of oscillatory feature above the edge to become Cu_3P. It is found that Cu_3P forms at the expense of Cu^0 which diminishes at 620 °C.

In contrast, XANES spectra of $Cu_2P_2O_7$/USY evolve differently. As illustrated in Fig. 7b, several trends can be seen. The structural transformation from $Cu_2P_2O_7$ to Cu_3P seems to proceed through several reaction steps, in accordance with *in situ* XRD results. Although quantitative analysis could not be performed due to a lack of reference spectra of metastable intermediate phases, a close inspection of XANES spectra reveals the first phase transformation at temperatures above 220 °C. The white line intensity gradually decreases, a characteristic shoulder of Cu0 emerges at ~ 8981 eV, and the edge progressively shifts to ~ 8979 eV (at 450 °C). This modification of spectral features indicates the reduction of $Cu_2P_2O_7$ (Cu^{2+}) to Cu0 metal which takes place at a temperature lower than that of $Cu_2P_2O_7/SiO_2$ precursor. This result is in good agreement with H_2-TPR and *in situ* XRD analyses. When the temperature increases from 450 to 650 °C, the spectral features evolve toward the Cu_3P structure through several intermediate phases, as different trends of oscillation alteration are observed. In general, the

Table 1
The %Conversion of oleic acid and the %Yield of products measured at 340 °C for 6 h.

Percentage	Cu_3P/USY	Cu_3P/SiO_2
Conversion	99.99	99.99
Yield		
- Heptadecane ($C_{17}H_{36}$)	–	–
- Octadecane ($C_{18}H_{38}$)	–	–
- Dodecylbenzene ($C_{18}H_{30}$)	32.84	46.13
- Dodecylcyclohexane ($C_{18}H_{36}$)	8.31	4.55
- Heptylcyclopentane ($C_{12}H_{24}$)	5.01	–
- Others	53	49

structural evolutions of all supported catalysts deduced from *in situ* XAS spectra are consistent with *in situ* XRD results. A slight discrepancy in phase transformation temperatures observed by both techniques is possibly related to the different increments of temperature. As XRD measurement required relatively long data collection times, diffraction patterns were recorded every 50 °C, while time-resolved XAS spectra were collected every 10 °C. An alternative explanation for this discrepancy may be the ability of XAS to obtain local structural information on both the crystalline and amorphous nanoparticles. It seems likely that XAS can probe amorphous particles or very small nanoparticles which may occur before the formation of nanocrystalline phases detected by XRD.

In summary, *in situ* XRD and *in situ* XAS give complementary structural information. *In situ* XRD provides insights into the crystal structure transformation process while *in situ* XAS provides the information on the evolution of the valence states and the local atomic structures of Cu during hydrogen reduction of $Cu_2P_2O_7$ to Cu_3P nanoparticles on SiO_2 and USY supports. Both techniques revealed that the formation mechanism of Cu_3P consists of multiple reaction steps. The $Cu_2P_2O_7$ precursor is first reduced to metallic Cu which can facilitate the dissociation of hydrogen molecules to hydrogen atoms. The hydrogen spillover may occur and assist the reduction of phosphate to volatile phosphorus compounds, *i.e.*, PH_3 and H_3PO_4 [1,4,17,25] which later react with metallic Cu to form Cu_3P on SiO_2 support. In contrast, the reduced Cu particles on USY support partially transform to CuP_2 and $Cu(OH)_2$ before all converting to Cu_3P. It is also found that the nature of catalyst supports exerts a significant influence on the reduction behavior of $Cu_2P_2O_7$ catalyst. From the *in situ* XAS results that were collected every 10 °C, the onset reduction temperature of $Cu_2P_2O_7$/USY (~ 230 °C) is much lower than that of $Cu_2P_2O_7/SiO_2$ (~ 320 °C). This can be explained by the fact that $Cu_2P_2O_7$ might exhibit a stronger interaction with SiO_2 support, as small amounts of SiP_2O_7 is also formed during the reaction. Moreover, the ultra-stable zeolite Y (USY) support is known to have higher acidity than SiO_2 support, which may result in a high efficiency of spilled over hydrogen diffusion enhancing the reduction of $Cu_2P_2O_7$ [32]. The $Cu_2P_2O_7$/USY is therefore more easily reduced than the other support, possibly enabling the formation of Cu_3P with smaller particle size.

3.4. Catalytic deoxygenation of oleic acid

Conversion of oleic acid and deoxygenation (DO) yields of supported Cu_3P catalysts are listed in Table 1. At the collecting time of 6 h, each catalyst reaches a complete conversion. Both Cu_3P/SiO_2 and Cu_3P/USY catalysts exhibit similar catalytic behavior. Oleic acid is transformed to cyclic and aromatic compounds through cyclization and aromatization. The main product is dodecylbenzene while dodecylcylclohexane is a minor product. Cu_3P/SiO_2 achieves higher dodecylbenzene yield (46 %) than Cu_3P/USY (33 %). The lower selectivity of Cu_3P/USY is possibly due to the higher acidity of USY support [23,33,34] that may favor cracking reaction, giving heptylcyclopentane as a by-product. In this case, support appears to exert influence over the product selectivity but not the reaction mechanism of the Cu_3P catalyst.

It is worth noting that Cu_3P catalyst provides different reaction mechanism compared to other metal phosphide catalysts, such as CoP, Ni_2P, WP, MoP, FeP, which have been reported to favor deoxygenation of oxygenated compounds to alkanes [1–7]. Additionally, different supports may possess different structure, different Lewis acid sites (metal sites) and Brönsted sites (P–OH sites) of metal phosphides that may affect their intrinsic activities [2,33,34]. Therefore, the supported Cu_3P catalysts can have potential applications in the valorization of vegetable oil or biofuel for the production of cyclic and aromatic compounds.

According to the analysis of catalytic results in Table 1, a plausible mechanism for the deoxygenation of oleic acid over supported Cu_3P catalysts could be summarized in Scheme 1. This proposed mechanism is based on the surface reaction. It can be seen that supported Cu_3P

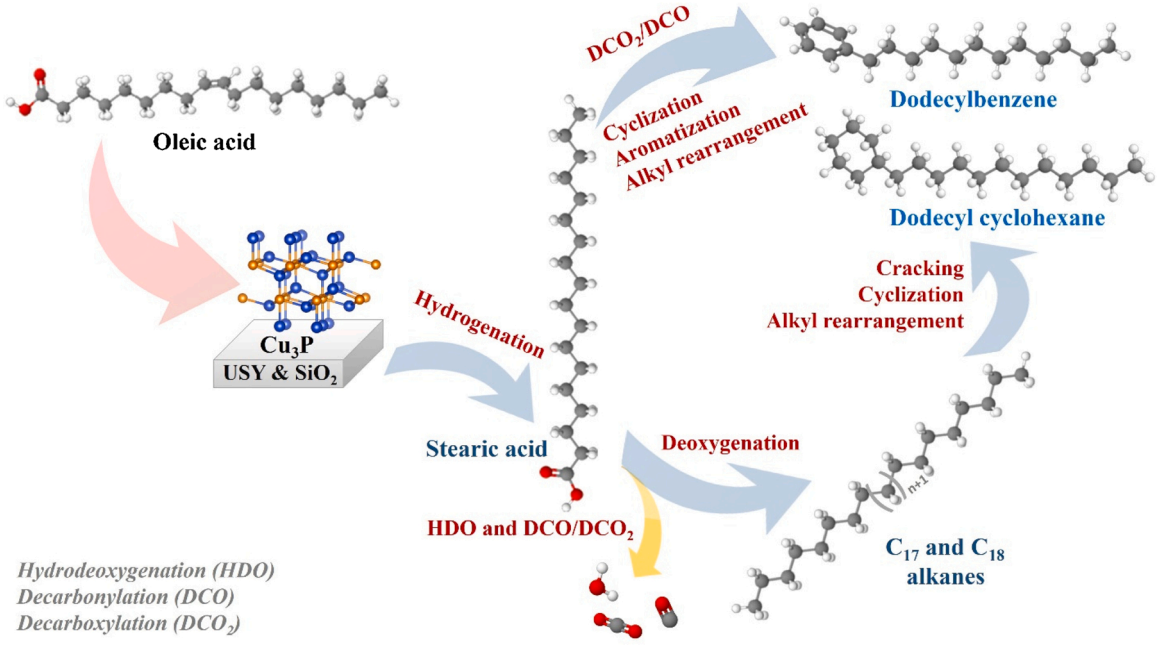

Scheme 1. Proposed mechanism for the deoxygenation of oleic acid over supported Cu_3P.

catalysts favor the hydrogenation of oleic acid to form stearic acid. Then, there are two further main reaction pathways. The first one starts with cracking of stearic acid, cyclization, aromatization, and alkyl rearrangement. This pathway gives dodecylbenzene as a final product. The second one starts with the removal of H_2O, CO and CO_2 from stearic acid, followed by cracking, cyclization and alkyl rearrangement. This pathway could provide dodecyl cyclohexane as the final product.

4. Conclusion

Cu_3P catalysts supported on SiO_2 and ultra-stable zeolite Y (USY) were successfully prepared by hydrogen reduction of copper pyrophosphate precursor ($Cu_2P_2O_7$). The phase transition was monitored by H_2-TPR, *in situ* XRD and XAS. The combination of these techniques was proven to be a powerful tool to understand the formation mechanism of supported metal phosphide nanoparticles and the influence of the support materials on the reaction mechanism. Several phase transformations were observed. The $Cu_2P_2O_7$ precursor was reduced to metallic Cu, which later reacted with volatile phosphorus compounds and directly transformed to Cu_3P particles on SiO_2 support, whereas the reduced Cu on USY support evolved through CuP_2 and $Cu(OH)_2$ intermediates before transforming to Cu_3P. The reduction of $Cu_2P_2O_7$ to Cu_3P on USY seemed to be more facile compared to that on SiO_2, although it proceeded through multiple steps. It exhibited the lowest onset reduction temperature and provided Cu_3P having a smaller particle size. The Cu_3P supported catalysts were demonstrated to achieve a high conversion of almost 100 % for deoxygenation of oleic acid. Both Cu_3P/SiO_2 and Cu_3P /USY catalysts favored cyclization and aromatization to form cyclic and aromatic compounds. Cu_3P/SiO_2 achieved higher dodecylbenzene yield (46 %) than Cu_3P/USY (33 %). The catalyst support appeared to exert influence over the product selectivity but not the reaction mechanism of the Cu_3P catalyst. Cu_3P could be considered as a promising catalyst for the valorization of vegetable oil or biofuel for the production of cyclic and aromatic compounds. The information obtained from this study could be used to optimize conditions for the production of supported Cu_3P nanopartcles for catalytic applications.

CRediT authorship contribution statement

Nopparuj Kochaputi: Writing - original draft. **Pongtanawat Khemthong:** Conceptualization, Writing - review & editing. **Teera Butburee:** Writing - review & editing. **Sanchai Kuboon:** Writing - review & editing. **Kajornsak Faungnawakij :** Writing - review & editing. **Chanapa Kongmark:** Conceptualization, Writing - review & editing.

Declaration of Competing Interest

The authors report no declarations of interest.

Acknowledgements

This work was co-supported by Kasetsart University Research and Development Institute (KURDI) and National Nanotechnology Center (NANOTEC) through its program of Research Network NANOTEC (RNN). This work was also supported by National Science and Technology Development Agency (NSTDA) via CAS-NSTDA Project (P1952712) i. We also would like to thank Prof. Gopinathan Sankar and Attera Worayingyong for insightful advice and discussions. We are grateful to Prof. S. Seraphin (Professional Authorship Center, NSTDA) for fruitful discussions on manuscript editing. All authors also thank Mr. Chakrit Yimsukanan for his support.

References

[1] P. Bui, J.A. Cecilia, S.T. Oyama, A. Takagaki, A. Infantes-Molina, H. Zhao, D. Li, E. Rodríguez-Castellón, A.J. López, Studies of the synthesis of transition metal phosphides and their activity in the hydrodeoxygeblenation of a biofuel model compound, J. Catal. 294 (2012) 184–198, https://doi.org/10.1016/j.jcat.2012.07.021.

[2] M. Peroni, I. Lee, X. Huang, E. Baráth, O.Y. Gutiérrez, J.A. Lercher, Deoxygenation of palmitic acid on unsupported transition-metal phosphides, ACS Catal. 7 (2017) 6331–6341, https://doi.org/10.1021/acscatal.7b01294.

[3] H.Y. Zhao, D. Li, P. Bui, S.T. Oyama, Hydrodeoxygenation of guaiacol as model compound for pyrolysis oil on transition metal phosphide hydroprocessing catalysts, Appl. Catal. A Gen. 391 (2011) 305–310, https://doi.org/10.1016/j.apcata.2010.07.039.

[4] R. Prins, M.E. Bussell, Metal phosphides: preparation, characterization and catalytic reactivity, Catal. Lett. 142 (2012) 1413–1436, https://doi.org/10.1007/s10562-012-0929-7.

[5] J.A. Cecilia, A. Infantes-Molina, E. Rodríguez-Castellón, A. Jiménez-López, S. T. Oyama, Oxygen-removal of dibenzofuran as a model compound in biomass derived bio-oil on nickel phosphide catalysts: role of phosphorus, Appl. Catal. B 136 (2013) 140–149, https://doi.org/10.1016/j.apcatb.2013.01.047.

[6] J.-S. Moon, E.-G. Kim, Y.-K. Lee, Active sites of Ni_2P/SiO_2 catalyst for hydrodeoxygenation of guaiacol: a joint XAFS and DFT study, J. Catal. 311 (2014) 144–152, https://doi.org/10.1016/j.jcat.2013.11.023.

[7] N. Kochaputi, C. Kongmark, P. Khemthong, T. Butburee, S. Kuboon, A. Worayingyong, K. Faungnawakij, Catalytic behaviors of supported Cu, Ni, and Co phosphide catalysts for deoxygenation of oleic acid, Catalysts 9 (2019) 715, https://doi.org/10.3390/catal9090715.

[8] R. Wang, X.-Y. Dong, J. Du, J.-Y. Zhao, S.-Q. Zang, MOF-derived bifunctional Cu_3P nanoparticles coated by a N, P-codoped carbon shell for hydrogen evolution and oxygen reduction, Adv. Mater. 30 (2018) 1703711, https://doi.org/10.1002/adma.201703711.

[9] L. Ma, X. Shen, H. Zhou, J. Zhu, C. Xi, Z. Ji, L. Kong, Synthesis of Cu_3P nanocubes and their excellent electrocatalytic efficiency for the hydrogen evolution reaction in acidic solution, RSC Adv. 6 (2016) 9672–9677, https://doi.org/10.1039/C5RA24427G.

[10] C.-C. Hou, Q.-Q. Chen, C.-J. Wang, F. Liang, Z. Lin, W.-F. Fu, Y. Chen, Self-supported cedarlike semimetallic Cu_3P nanoarrays as a 3D high-performance Janus electrode for both oxygen and hydrogen evolution under basic conditions, ACS Appl. Mater. Interfaces 8 (2016) 23037–23048, https://doi.org/10.1021/acsami.6b06251.

[11] T. Soták, T. Schmidt, M. Hronec, Hydrogenolysis of polyalcohols in the presence of metal phosphide catalysts, Appl. Catal. A Gen. 459 (2013) 26–33, https://doi.org/10.1016/j.apcata.2013.04.006.

[12] L. De Trizio, A. Figuerola, L. Manna, A. Genovese, C. George, R. Brescia, Z. Saghi, R. Simonutti, M. Van Huis, A. Falqui, Size-tunable, hexagonal plate-like Cu_3P and janus-like Cu-Cu_3P nanocrystals, ACS Nano 6 (2012) 32–41, https://doi.org/10.1021/nn203702r.

[13] S. Carenco, D. Portehault, C. Boissière, N. Mézailles, C. Sanchez, Exploring nanoscaled matter from speciation to phase diagrams: metal phosphide nanoparticles as a case of study, Adv. Mater. 26 (2014) 371–390, https://doi.org/10.1002/adma.201303198.

[14] M.-P. Bichat, T. Politova, H. Pfeiffer, F. Tancret, L. Monconduit, J.-L. Pascal, T. Brousse, F. Favier, Cu_3P as anode material for lithium ion battery: powder morphology and electrochemical performances, J. Power Sources 136 (2004) 80–87, https://doi.org/10.1016/j.jpowsour.2004.05.024.

[15] S. Liu, Y. Qian, L. Xu, Synthesis and characterization of hollow spherical copper phosphide (Cu_3P) nanopowders, Solid State Commun. 149 (2009) 438–440, https://doi.org/10.1016/j.ssc.2008.12.046.

[16] H. Pfeiffer, F. Tancret, T. Brousse, Synthesis, characterization and electrochemical properties of copper phosphide (Cu_3P) thick films prepared by solid-state reaction at low temperature: a probable anode for lithium ion batteries, Electrochim. Acta 50 (2005) 4763–4770, https://doi.org/10.1016/j.electacta.2005.02.024.

[17] C. Stinner, Z. Tang, M. Haouas, Th. Weber, R. Prins, Preparation and ^{31}P NMR characterization of nickel phosphides on silica, J. Catal. 208 (2002) 456–466, https://doi.org/10.1006/jcat.2002.3577.

[18] G. Berhault, P. Afanasiev, H. Loboué, C. Geantet, T. Cseri, C. Pichon, C. Guillot-Deudon, A. Lafond, In situ XRD, XAS, and magnetic susceptibility study of the reduction of ammonium nickel phosphate $NiNH_4PO_4{\cdot}H_2O$ into nickel phosphide, Inorg. Chem. 48 (2009) 2985–2992, https://doi.org/10.1021/ic802074k.

[19] J.A. Rodriguez, J.-Y. Kim, J.C. Hanson, S.J. Sawhill, M.E. Bussell, Physical and chemical properties of MoP, Ni_2P, and MoNiP hydrodesulfurization catalysts: time-resolved X-ray diffraction, density functional, and hydrodesulfurization activity studies, J. Phys. Chem. B 107 (2003) 6276–6285, https://doi.org/10.1021/jp022639q.

[20] H. Shi, J. Chen, Y. Yang, S. Tian, Catalytic deoxygenation of methyl laurate as a model compound to hydrocarbons on nickel phosphide catalysts: remarkable support effect, J. Catal. 208 (2002) 456–466, https://doi.org/10.1006/jcat.2002.3577.

[21] Y. Poo-arporn, P. Chirawatkul, W. Saengsui, S. Chotiwan, S. Kityakarn, S. Klinkhieo, J. Hormes, P. Songsiriritthigul, Time-resolved XAS (Bonn-SUT-SLRI) beamline at SLRI, J. Synchrotron Rad. 19 (2012) 937–943, https://doi.org/10.1107/S090904951204109X.

[22] B. Ravel, M. Newville, ATHENA, ARTEMIS, HEPHAESTUS: data analysis for X-ray absorption spectroscopy using IFEFFIT, J. Synchrotron Rad. 12 (2005) 537–541, https://doi.org/10.1107/S0909049505012719.

[23] H. Zuo, Q. Liu, T. Wang, L. Ma, Q. Zhang, Q. Zhang, Hydrodeoxygenation of methyl palmitate over supported Ni catalysts for diesel-like fuel production, Energy Fuels 26 (2012) 3747–3755, https://doi.org/10.1021/ef300063b.

[24] T.C. Vaimakis, A.T. Sdoukos, The thermal dehydration of the $Ca(H_2PO_4)_2{\cdot}H_2O$-SiO_2 system. Part 1. Mechanism, Thermochim. Acta 277 (1996) 107–120, https://doi.org/10.1016/0040-6031(95)02751-3.

[25] X. Lan, E.J.M. Hensen, T. Weber, Silica-supported Ni_2P: Effect of preparation conditions on structure and catalytic performance in thiophene hydrodesulfurization (HDS), Catal. Today 292 (2017) 121–132, https://doi.org/10.1016/j.cattod.2016.12.040.

[26] H. Schlenqer, H. Jacobs, R. Juza, Ternäre phasen des lithiums mit kupfer und phosphor, Z. Anorg. Allg. Chem. 385 (1971) 177–201, https://doi.org/10.1002/zaac.19713850302.

[27] J.-H. Chen, K.H. Whitmire, A structural survey of the binary transition metal phosphides and arsenides of the d-block elements, Coord. Chem. Rev. 355 (2018) 271–327, https://doi.org/10.1016/j.ccr.2017.08.029.

[28] M. Staniuk, D. Zindel, W. van Beek, O. Hirsch, N. Kränzlin, M. Niederberger, D. Koziej, Matching the organic and inorganic counterparts during nucleation and growth of copper-based nanoparticles – in situ spectroscopic studies, CrystEngComm 17 (2015) 6962–6971, https://doi.org/10.1039/c5ce00454c.

[29] L.-S. Kau, D.J. Spira-Solomon, J.E. Penner-Hahn, K.O. Hodgson, E.I. Solomon, X-ray absorption edge determination of the oxidation state and coordination number of copper: application to the type 3 site in Rhus vernicifera Lacease and its reaction with oxygen, J. Am. Chem. Soc. 109 (1987) 6433–6442, https://doi.org/10.1021/ja00255a032.

[30] S. Pithakratanayothin, R. Tongsri, T. Chaisuwan, S. Wongkasemjit, P. Khemthong, S. Limpijumnong, P. Pharanchai, K. Malaicharoen, Discovery of mono(u-oxo) dicopper and bis(u-oxo)dicopper in ordered Cu incorporated in SBA-15 via sol-gel process from silatrane at room temperature: an in situ XAS investigation, Microporous Mesoporous Mater. 301 (2020) 110225, https://doi.org/10.1016/j.micromeso.2020.110225.

[31] P. Khemthong, P. Photai, N. Grisdanurak, Structural properties of CuO/TiO_2 nanorod in relation to their catalytic activity for simultaneous hydrogen production under solar light, Int. J. Hydrogen Energy 38 (2013) 15992–16001, https://doi.org/10.1016/j.ijhydene.2013.10.065.

[32] P.S.F. Mendes, G. Lapisardi, C. Bouchy, M. Rivallan, J.M. Silva, M.F. Ribeiro, Hydrogenating activity of Pt/zeolite catalysts focusing acid support and metal dispersion influence, Appl. Catal. A Gen. 504 (2015) 17–28, https://doi.org/10.1016/j.apcata.2015.03.027.

[33] M. Breysse, P. Afanasiev, C. Geantet, M. Vrinat, Overview of support effects in hydrotreating catalysts, Catal. Today 86 (2003) 5–16, https://doi.org/10.1016/S0920-5861(03)00400-0.

[34] Y. Zheng, J. Wang, C. Liu, Y. Lu, X. Lin, W. Li, Z. Zheng, Efficient and stable Ni-Cu catalysts for ex situ catalytic pyrolysis vapor upgrading of oleic acid into hydrocarbon: Effect of catalyst support, process parameters and Ni-to-Cu mixed ratio, Renew. Energy 154 (2020) 797–812, https://doi.org/10.1016/j.renene.2020.03.058.